Surface aggregate morphology of chiral porphyrins as a function of constitution and amphiphilic nature†

Patrizia Iavicoli, Maite Simón-Sorbed and David B. Amabilino*

Received (in Montpellier, France) 2nd September 2008, Accepted 27th October 2008
First published as an Advance Article on the web 16th December 2008
DOI: 10.1039/b815177f

The deposition of molecules onto surfaces from dilute solutions can lead to a variety of layer morphologies depending on the balance of interactions between solvent and molecule, molecules themselves, and these two components and the surface. Here we explore the behaviour of a set of chiral tetra *meso*-amidophenyl-substituted porphyrins—containing long hydrophobic tails at the periphery of the conjugated π-electron system—after depositing a drop of each compound from different solutions onto graphite. The synthesis of the new compounds is detailed and the morphology of the aggregates they form on the substrate has been investigated by atomic force microscopy (AFM). Depending on the solvent used and composition and constitution of the compound the structures formed are very different. Round shape aggregates and larger dewetting type patterns were formed from solutions of the compounds in methanol—in which all the molecules exhibit non-specific aggregation—and when chloroform and toluene are used fibril-like structures appear, whose alignment with the graphite axes depends on the length of the alkyl chains attached to the amide moiety in the molecules.

Introduction

Porphyrins are attractive components in molecular materials for a number of reasons, including the transfer of charge where a number of groups, notably including that of Jean-Pierre Sauvage, have made important discoveries concerning electron transfer.[1–10] These studies, inspired by the photosynthetic reaction centre,[11] have helped towards understanding the phenomenon within relatively large molecules, but another important area is that of the transport of charge in much larger aggregates.[12–15] In this sense, the preparation of synthetic assemblies on surfaces[16,17] and the study of properties such as photoconductivity are important areas of activity.[18,19]

While many of the subtle mechanisms governing the aggregation of molecular species in solution have been unravelled,[20–25] the understanding of the way molecules come together at surfaces is still very limited:[26–27] The formation of self-ordered nanostructures at surfaces is more complicated than in solution as it requires the additional control over interactions of either molecules or their aggregates with the surface. In addition, the packing of the first layer can be different from that of the subsequent layers because of the interaction of the molecule with the surface.[28,29] A deeper understanding of the assembly of different compounds at various surfaces under different conditions is crucial to achieve full control over the growth of aggregates across multiple length scales of functional architectures with desired structure and properties.[26]

As part of an ongoing project to investigate the role of hydrogen bonds in the aggregation of aromatic systems at surfaces, we chose to prepare and study the tetra-*meso*-amidophenyl-substituted porphyrin derivative **1** (Fig. 1). This compound gives a variety of different superstructures at the surface depending on the solvent used upon casting the molecule on the substrate, as shown by acoustic mode atomic force microscopy (AFM), after depositing a drop of a solution of the compound on the freshly cleaved substrate (either graphite or mica) and allowing the solvent to evaporate.[30] It was demonstrated how different solvents can modify the interactions of the molecule with itself and with the surface.

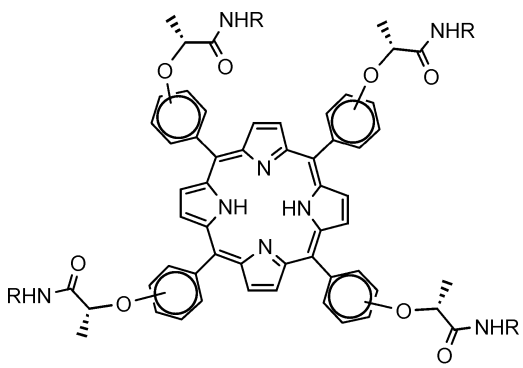

(*R,R,R,R*)-**1** 4-phenyl R = $C_{12}H_{25}$

(*R,R,R,R*)-**2** 3-phenyl R = $C_{12}H_{25}$

(*R,R,R,R*)-**3** 3-phenyl R = $C_{18}H_{37}$

(*R,R,R,R*)-**4** 4-phenyl R = $C_{18}H_{37}$

Fig. 1 Chemical structures of the compounds prepared in this work.

Institut de Ciència de Materials de Barcelona (CSIC), Campus Universitari de Bellaterra, 08193 Cerdanyola del Vallès Catalonia, Spain. E-mail: amabilino@icmab.es; Fax: +34 93 5805729; Tel: +34 93 5801853

† Dedicated to Prof. Jean-Pierre Sauvage on the occasion of his 65th birthday.

However, it is clear that non-covalent interactions are playing a very important role in the morphology of the films, which are new and intriguing. In an attempt to shed light on the key factors influencing the aggregate morphology, we have varied the molecular composition and constitution in order to explore the origins of these effects, and here we report our findings. Specifically, the series of novel porphyrin derivatives **2**–**4** (Fig. 1) was synthesized, where the number of carbon atoms in the alkyl chain and their position on the phenyl ring affect the self-assembly and the organization onto a surface.

We chose to study the molecules on a graphite surface, because the amide's ability to self-assemble functional units in fibre-like aggregates is disturbed on a hydrophilic surface, because of the possible interaction between the amide groups of the molecules with it, as seen for other amide derivatives.[31,32] The studies are distinct from those carried out under equilibrium conditions in solvent at the graphite surface[33,34] because kinetics and solvent evaporation play an important role in the formation of the nanostructures.[27] The alkyl chain can modify the morphology of aggregates because it changes the solubility, and the porphyrins substituted at the 3-position might be expected to hinder the formation of well defined aggregates because of the multiple conformers that exist for these compounds.

Results and discussion

1. Synthesis and characterisation

The porphyrins **1**–**4** were prepared by the synthetic route described in Scheme 1. In the first step 3- and 4-hydroxybenzaldehyde were condensed stereoselectively with (*S*)-methyl lactate in the presence of triphenylphosphine and diisopropylazodicarboxylate, as reported previously.[35,36] The resulting aldehydes **5** and **6** were then used in the condensation with pyrrole in refluxing propionic acid in air[37] to give the new corresponding porphyrin derivatives **7** and **8**. These compounds showed the characteristic spectroscopic data of tetraphenylporphyrin derivatives. The condensations of the esters with dodecylamine and octadecylamine were performed by heating the esters **7** and **8** at 80 °C using the amines as solvent. This procedure afforded the chiral amides **1**–**4** in respectable yields after thorough purification by column chromatography. Their structures were confirmed by all the habitual spectroscopic techniques and elemental analysis.

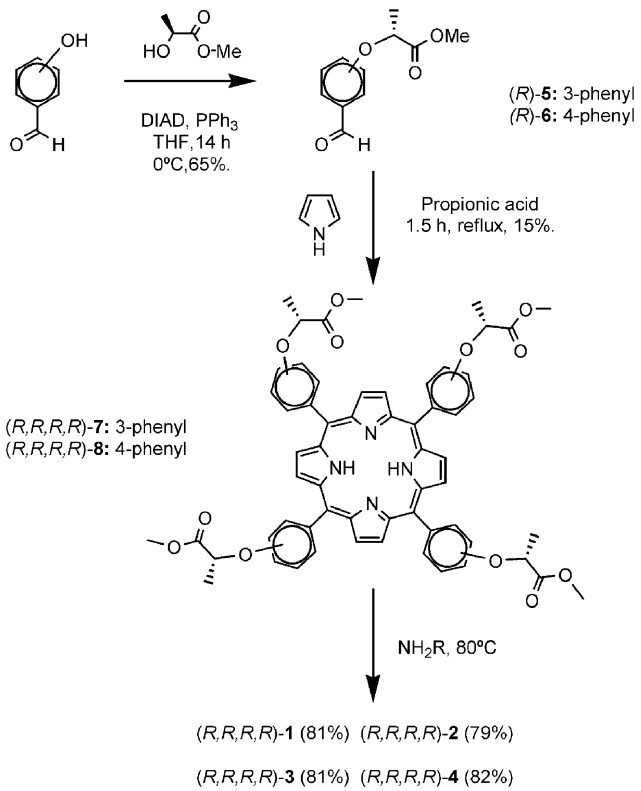

Scheme 1

2. Atomic force microscopy measurements

The morphologies of the aliphatic porphyrin aggregates at the air–substrate interface were studied by acoustic mode AFM after depositing a drop of a solution of the compounds on a freshly cleaved piece of highly oriented pyrolytic graphite (HOPG) substrate and allowing the solvent to evaporate. The technique is particularly appropriate for the study of this kind of aggregate because no treatment of the surface is necessary prior to imaging, which was always performed in ambient conditions.

Topographic AFM images of films of (*R*,*R*,*R*,*R*)-**2**—which has four dodecyl chains substituted at the 3-position of the phenyl groups—drop cast from different solvents onto HOPG are shown in Fig. 2–5. When the solution of the compound in methanol is cast onto the graphite surface, a typical dewetting phenomenon is observed whereby worm-like islands of material with no internal structure are formed (Fig. 2). A shattered monolayer around 2 nm thick can be observed with small layers a further 2 nm thick growing on top of it in places. In this solvent, it seems that the interactions between the surface and the molecules are not strong enough to dominate a specific film forming process. The diameter of a tetraphenylporphyrin is estimated to be 1.4 nm, the chain length 1.7 nm in this case, and the thickness is 0.4 nm. Therefore the total length of the porphyrin molecule core and the two opposite tails is 4.8 nm. If we assume the molecule to be perpendicular to the substrate with the chains extended away following the plane of the porphyrin ring, the distance between the methyl groups at the ends of two opposite chains is less than 4.8 nm. It therefore appears that the layers contain molecules with the porphyrin core oriented quasi-perpendicularly to the surface with the alkyl chains folded in an approximately parallel orientation to the surface.

When the solvent used is changed to chloroform (Fig. 2 and Fig. 3) the formation of needle like structures of between 6 and 10 nm thick (as judged from the *z*—vertical with respect to the flat surface—scale in the AFM image), around 40 nm wide and approximately 150 to 300 nm in length are formed. In this less polar solvent, well defined structures are formed partially thanks to the better interaction between molecules themselves and the substrate, as indicated upon Fourier transform of the images which reveals a clear preference for alignment of the acicular structures along the symmetry axes of the graphite (not shown). The image showing the smaller area (Fig. 3)

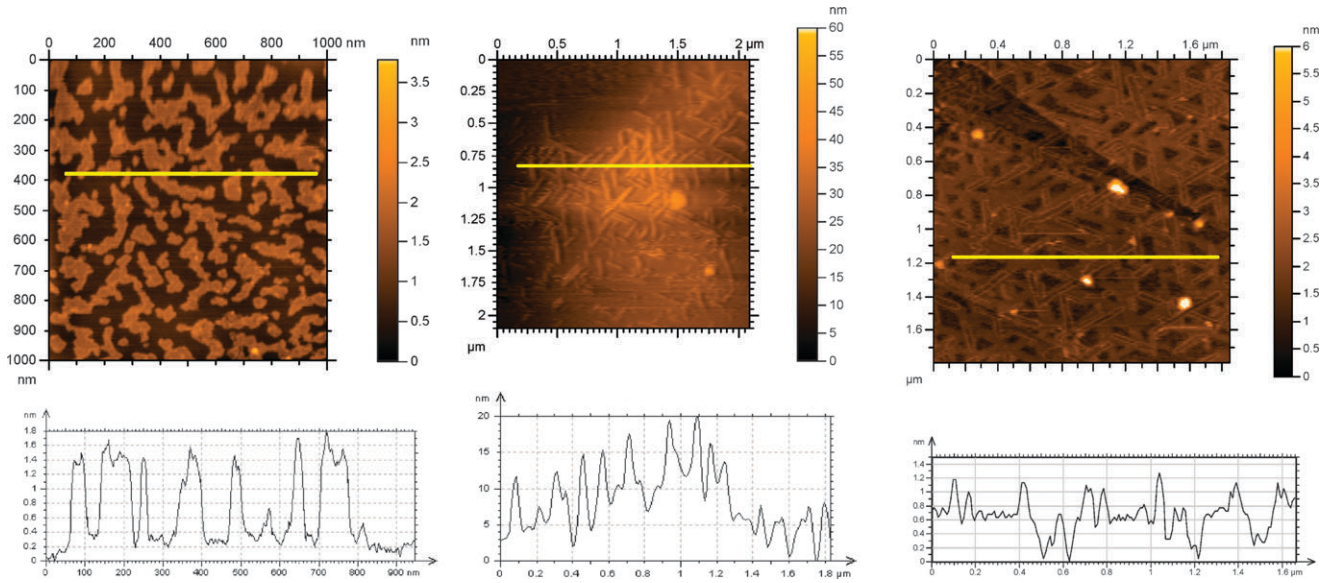

Fig. 2 Topographic AFM images of films of (*R*,*R*,*R*,*R*)-**2** drop cast onto HOPG from a 1×10^{-5} M solution in MeOH (left), chloroform (centre) and toluene (right). The contours in the frames below the images correspond to the line in the image.

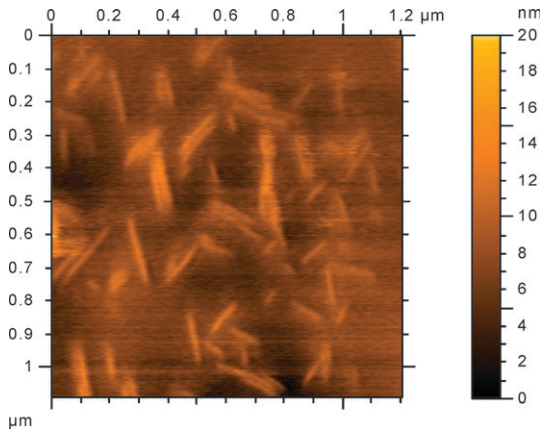

Fig. 3 Topographic AFM image of a film of (*R*,*R*,*R*,*R*)-**2** drop cast onto HOPG from a 1×10^{-5} M solution in $CHCl_3$.

clearly indicates some interaction between the fibres, as they are often seen in pairs or threes and have quite uniform width.

When (*R*,*R*,*R*,*R*)-**2** was deposited onto the graphite surface from toluene a range of different morphologies was observed, the most representative morphology being needle-like objects in which the border is higher than the centre (Fig. 2). The height of these borders is approximately 0.4 nm, and the longitudinal dimensions of the objects are between 100 and 300 nm and the distance between the rims is around 50 nm (Fig. 4). We are unaware of any report of such a structure upon deposition of an organic material on a surface. The orientation of the molecules is presumably planar to the surface because of the height. This situation also occurs in physisorbed monolayers in equilibrium on graphite where (*R*,*R*,*R*,*R*)-**4** is held to the surface by a combination of C–H···π interactions,[38] When this sample of (*R*,*R*,*R*,*R*)-**2** was heat annealed at about 50 °C for 2 h, the structure reorganised to give much larger tape-like objects (Fig. 5). Here, the apparent thickness is an average of 0.5 nm, with a

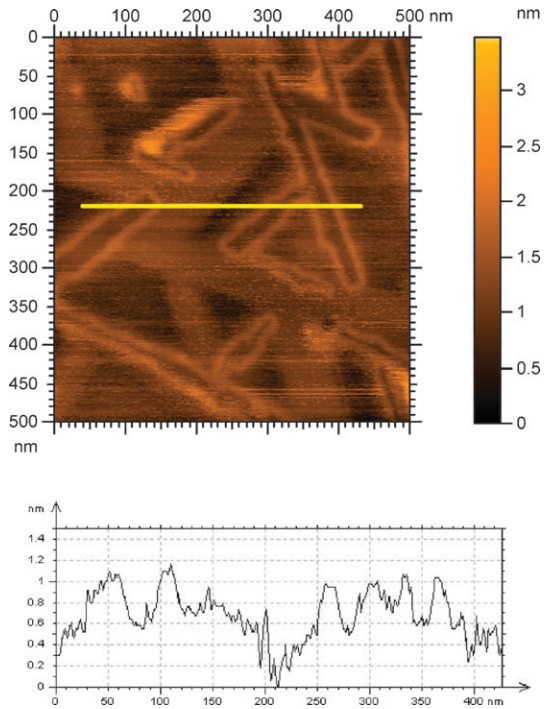

Fig. 4 Topographic AFM image of a film of (*R*,*R*,*R*,*R*)-**2** drop cast onto HOPG from a 1×10^{-5} M solution in toluene. The contour in the lower frame corresponds to the line in the image.

second layer whose surface is at a height of 1.4 nm above the graphite. This observation indicates that the layer in contact with the graphite is laying almost flat upon it, while the second layer is tilted up quasi-perpendicularly to the surface. This shows an interesting similarity to monolayers of a distinct porphyrin derivative which shows both flat and perpendicular arrangements relative to the surface within the monolayer.[39] Again, this low polarity solvent gives well defined structures, which in this case definitely lie flat on the surface and are

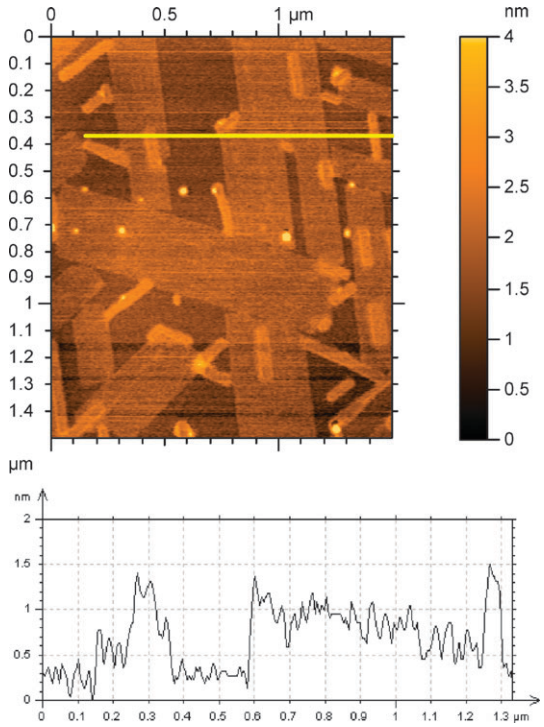

Fig. 5 Topographic AFM image of a film of (*R*,*R*,*R*,*R*)-**2** drop cast onto HOPG from a 1×10^{-5} M solution in toluene and heat annealed. The contour in the lower frame corresponds to the line in the image.

formed partially thanks to the better interaction between molecules themselves and the substrate, as indicated upon Fourier transform of the images, which reveals a clear preference for alignment along the symmetry axes of the graphite.

When (*R*,*R*,*R*,*R*)-**3**—which is identical to **2** with the exception that octadecyl chains are present instead of dodecyl chains—was deposited onto graphite from a methanol solution a complex morphology resulted (Fig. 6). At first sight, it appears that a dewetting pattern is the only one present, as for the shorter chain analogue. Yet closer inspection reveals that these areas of material are not uniform, but are pitted, and that in between them a much thinner layer of material is present. This situation can best be appreciated in the profiles of the layers shown in Fig. 6. The thinner layer has a maximum thickness of approximately 1 nm—consequent with a monolayer forming a very slight angle with the surface—while the dewetting shapes are approximately 8 nm thick (much larger than mono- or bilayer thickness), with pits going down to the monolayer height.

When (*R*,*R*,*R*,*R*)-**3** was deposited onto graphite from a chloroform solution, a complex web of short fibres of up to 1.5 nm high was formed (Fig. 6). The fact that the fibres overlapped each other and that they are oriented randomly strongly suggests that they are formed in solution and deposited as such onto graphite. A tilted orientation of the molecules with respect to the surface is thought to dominate in these objects. When the same molecule is deposited from a toluene solution, needles are formed (Fig. 6). The height of the objects is approximately 1.5 nm, which corresponds to the width of the tetraphenylporphyrin core, and the width and length of the fibres are 130–160 nm and 200–350 nm, respectively. The orientation of the fibres in this latter case is along the graphite axes.

The AFM images of films of the porphyrin (*R*,*R*,*R*,*R*)-**1** were reported in a previous correspondence.[28] Briefly, from chloroform the molecule forms very fine fibres on graphite and from toluene somewhat more well defined ones, very similar to those formed by (*R*,*R*,*R*,*R*)-**3**, while from methanol both these compounds show globular aggregates.

When compound (*R*,*R*,*R*,*R*)-**4** was deposited from MeOH solution onto the HOPG surface it showed the formation of round shaped aggregates of between 6 and 12 nm height (Fig. 7). Presumably, the methanol—which is a poor solvent for this highly apolar compound—favours the non-specific interaction between the molecules and, as a consequence of the small interaction with the substrate, round non-acicular aggregates are formed.

When a solution of (*R*,*R*,*R*,*R*)-**4** in toluene was deposited onto graphite areas of a smooth monolayer of 1.5 nm high are formed (Fig. 7). It can be observed that within some of these islands smaller needle shaped aggregates are present, whose length is between 200 and 300 nm, and the space between the centres of the well-defined fibres is between 30 and 60 nm. These fibres do seem to be aligned with the substrate symmetry directions. The length of the fully extended molecule is approximately 6 nm, and so they must be composed of several molecules. It is noteworthy, however, that less well resolved fibres are inferred in areas of the AFM images, which might correspond to single molecule wide fibres.

When the solution is changed to chloroform, long fibres of (*R*,*R*,*R*,*R*)-**4** with 1.5 nm height and 20–40 nm width are observed (Fig. 7). The fibres are very different from those observed in the previous cases, in that they are apparently isolated from each other and can be extremely long—up to a micron—and straight with no specific alignment to the graphite symmetry directions, indicating that the molecule–molecule interaction is higher than the molecule–surface interaction under these conditions. While the fibres are relatively straight, they do show definite kink points and more smoothly bent regions. In addition, there are areas in which bundles of fibres with multiple kinks are observed, and there are clear points at which fibres merge or diverge from one another. These characteristics correspond to a polymer type structure, and indicate that the molecule has formed a non-covalent chain of molecules with considerable rigidity, and that chains a single molecule wide are being imaged (since the convolution of the AFM tip gives a larger value of the width of the fibres than the actual one). This molecule and solvent combination is therefore unique amongst the ones studied in this work.

Discussion

A wide variety of surface morphologies have been observed for the four porphyrins and for the different conditions under which they were deposited onto the graphite surface. The solvent certainly plays a role in the aggregation of all the porphyrins which have been studied here, as has been observed in different systems, although the trends are different, presumably because of the different chemical composition and flexibility of the molecules. The more polar solvent—methanol,

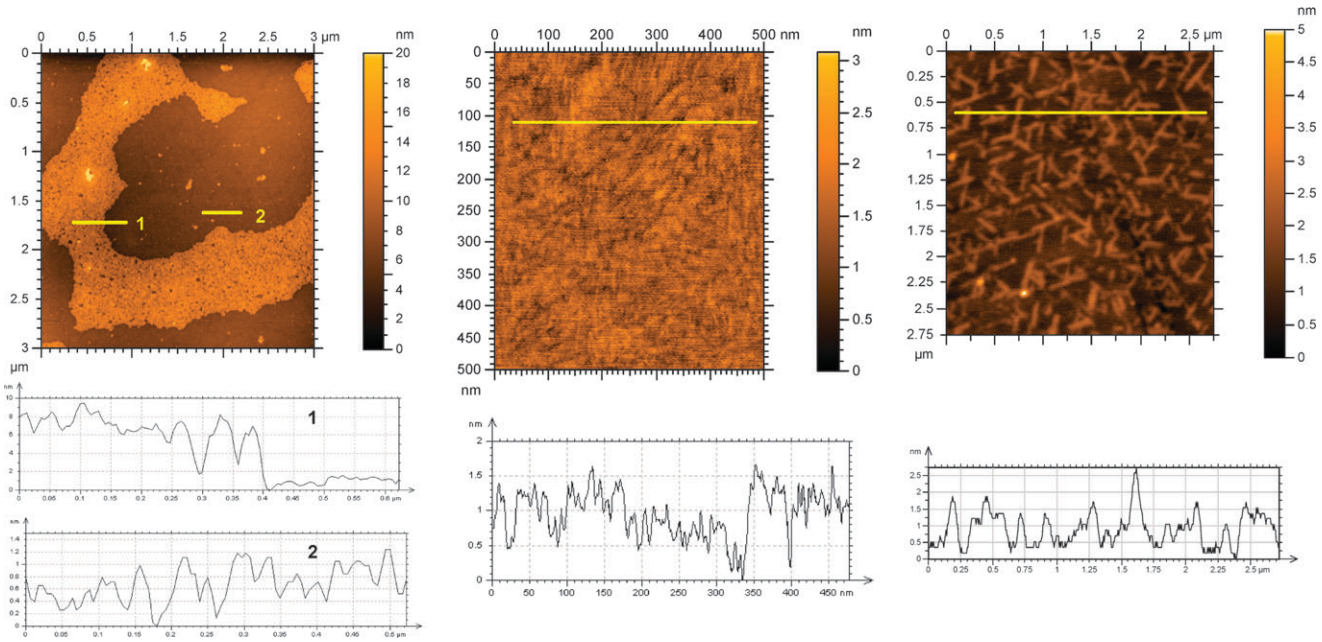

Fig. 6 Topographic AFM images of films of (*R*,*R*,*R*,*R*)-**3** drop cast onto HOPG from a 1×10^{-5} M solution in methanol (left), chloroform (centre) and toluene (right). The contours correspond to the lines in the images above them.

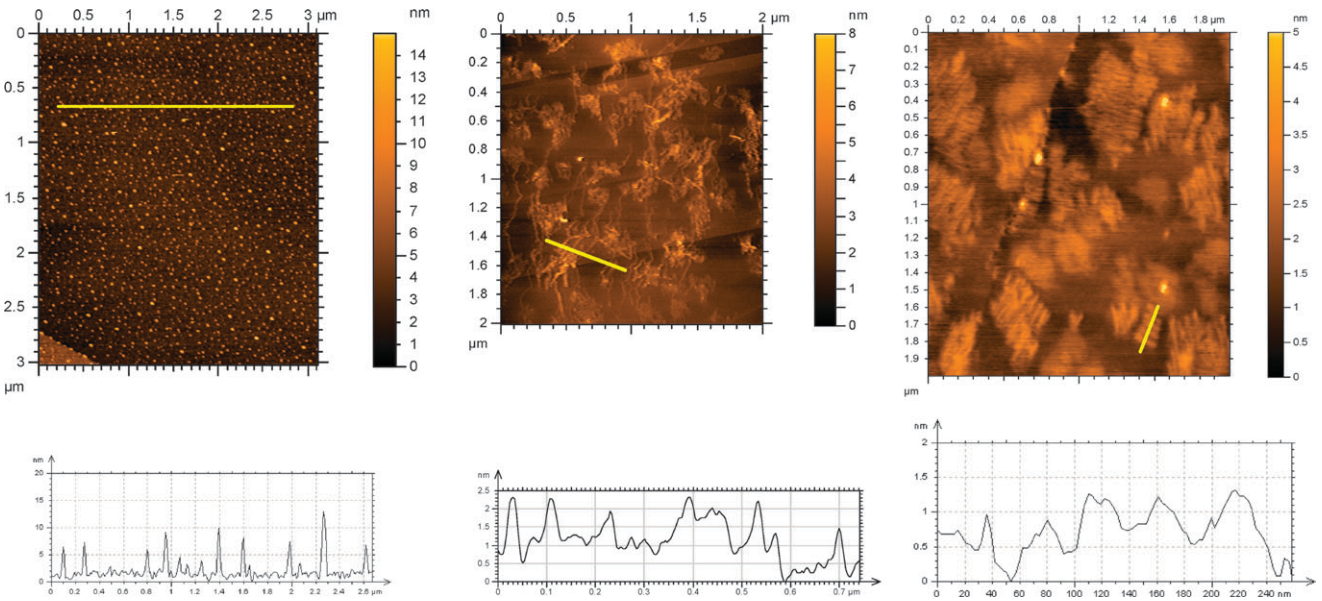

Fig. 7 Topographic AFM images of films of (*R*,*R*,*R*,*R*)-**4** drop cast onto HOPG from a 1×10^{-5} M solution in methanol (left), chloroform (centre) and toluene (right). The contours correspond to the lines in the images above them.

which is a poor solvent for the molecules and also a better hydrogen bond donor than the others—promotes non-specific molecule–molecule interactions with a consequent dewetting phenomenon being dominant in the layer formation, as observed in the AFM topography images of the samples. This aggregation in methanol was confirmed by UV-visible absorption spectroscopy, where a clear shift in the absorption bands is observed for methanol solutions (Fig. 8 for (*R*,*R*,*R*,*R*)-**3**, the other compounds show essentially the same difference in methanol) when compared with the spectra in either chloroform or toluene. Besides, methanol scarcely possesses an affinity for the apolar graphite surface compared with the other solvents, which presumably aids in favouring the adsorption of the porphyrin molecules into poorly ordered assemblies, such as the amorphous thin dewetting we observed. The longer alkyl chains seem to favour the formation of smaller structures at the surface, evidenced by the smaller globular type structures seen for **3** (in part) and **4**.

The less polar solvents, with a lower ability to form hydrogen bonds but greater ability to solvate the apolar parts of the molecules, apparently induce more specific intermolecular interactions between the amide groups in the molecules,

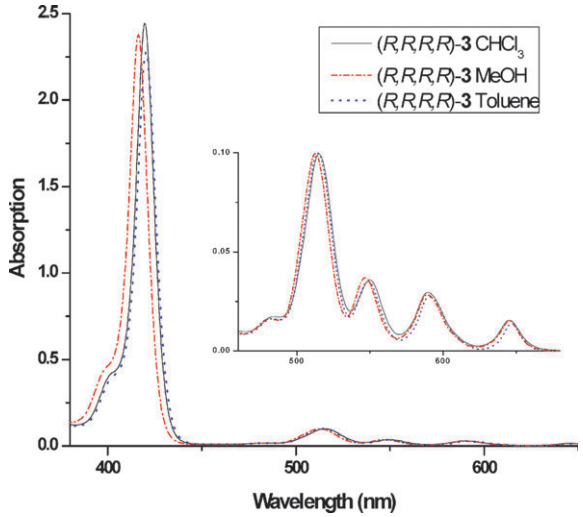

Fig. 8 UV-Vis absorption spectra of (*R*,*R*,*R*,*R*)-**3** in 5×10^{-6} M solutions in methanol, chloroform and toluene.

leading to the formation of fibril-like structures. In addition they seem to lead to a favourable interaction of the molecules with the apolar graphite surface, as revealed by the alignment of the fibres with the axes of the substrate, and avoid the kinetically driven (trapped) adsorption of porphyrins into the amorphous layer on the surface. The one exception in which the fibres do not follow the graphite axes is that of **4**, and here the porphyrins presumably preorganise in solution phase by hydrogen bonds and π–π interactions and produce columnar oligomers of molecules, which make the edge-on stacking style favourable when assembled on a solid substrate. Thus the planes of the porphyrins could be tilted from or perpendicular to the substrate. When the alkyl chain is longer, a better interaction with the surface stabilizes the structures and a tilted orientation of the porphyrin with respect to the surface plane is favoured.

Conclusions

The series of chiral tetra(alkylamidophenyl)-substituted porphyrins described here can be synthesized readily, and their self-assembly on graphite shows the dramatic role that solvent and composition can have on the film morphology, as revealed by the AFM studies. There is no evidence that the chirality of the molecule is expressed in the aggregates that are formed at the surface of the graphite, although it should be stated that any helicity within single fibres would be below the resolution limit of the AFM tips used in the experiments performed by us. The results do not rule out the utility of the porphyrins described here as chiral materials.[41]

The octadecyl chains favour greatly the formation of fibril-like structures when compared with the dodecyl counterparts. While the 4-substituted phenyl group might be expected to favour greatly the formation of ordered structures compared with the 3-phenyl compound (because of the multiple conformational isomers that exist for the latter), the effect here is not dramatic, although the 4-phenyl derivatives in general seem to organise better. These observations underline the importance of the dispersion interactions between the alkyl chains which can overcome unfavourable conformations and ensure aggregation, the octadecyl chain being particularly useful.

The compounds can form quite well ordered linear structures on graphite along the symmetry axes of the substrate, indicating that both molecule–molecule and molecule–substrate interactions are involved.[40] This situation arises only when non-polar solvents are used. The only case where alignment with the surface symmetry directions is not observed is when strong molecule–molecule interactions arise, in the case of **4**, where long fibril architectures are observed. It is hoped that these architectures and those derived from them can be exploited as active components for applications in various fields including (opto)electronics, photovoltaics, magnetism, and catalysis.

Experimental section

General details

The starting materials were purchased commercially and were used without further purification. Thin-layer chromatography (TLC) was performed on aluminium plates coated with Merck silica gel 60 F254. Developed plates were air-dried and scrutinized under a UV lamp. Silica gel 60 (35–70 mesh, SDS) was used for column chromatography. Melting points were determined by differential scanning calorimetry (DSC) using a Perkin Elmer DSC 7 instrument. LDI-TOF-MS were obtained using a Kratos Kompact Maldi 2 K-probe (Kratos Analytical) operating with pulsed extraction of the ions in linear high power mode. The samples were deposited directly onto a non-polished stainless steel sample plate from dichloromethane solution. ^{1}H and ^{13}C NMR spectra were recorded using the deuterated solvent as lock and tetramethylsilane as internal reference. Coupling constants are in Hertz. Compounds (*R*)-**5**,[29] (*R*)-**6**,[30] (*R*,*R*,*R*,*R*)-**4** and (*R*,*R*,*R*,*R*)-**8**[34] were prepared as described previously.

Synthesis

5,10,15,20-Tetra[3-(*R*,*R*,*R*,*R*)-methyl 2-phenoxypropanoate]-porphyrin ((*R*,*R*,*R*,*R*)-7). Freshly distilled pyrrole (266 μL, 3.84 mmol) and (*R*)-methyl 2-(3-formylphenoxy)propanoate (800 mg, 3.84 mmol) were added to refluxing propionic acid (14 mL) in air. After refluxing for 90 min, the solution was cooled to room temperature and the propionic acid was removed by careful evaporation *in vacuo*. The dark viscous material remaining was then washed thrice with hot water to remove remaining propionic acid and other undesired tar. The crude product was subjected to column chromatography on silica gel with CH_2Cl_2–MeOH (100 : 0.5) giving (*R*,*R*,*R*,*R*)-**7** as a purple solid (600 mg, 15% yield). **MF**: $C_{60}H_{54}N_4O_{12}$; **MW**: 1022.37; **LDI-TOF/MS** *m*/*z* (%): 1022.65 (100) $[M]^+$; **^{1}H NMR** (250 MHz, $CDCl_3$): 8.84 (dd, J = 3.9, 8H, pyrrole CH), 7.82 (d, J = 7.3, 4H, ArH), 7.71 (s, 4H, ArH), 7.63 (t, J = 7.5, 4H, ArH), 7.31 (d, J = 7.9, 4H, ArH), 4.97 (q, J = 6.9, 4H, ArO*CH*CH_3COOMe), 3.78 (s, 12H, ArOCHCH_3COO*Me*), 1.71 (d, J = 6.7, 12H, ArOCH*CH_3*COOMe), −2.87 (s, 8H, pyrrole NH) ppm; **FT-IR** (KBr): 2992 (w, CH_3), 2949 (w, CH_3), 1756 (s, CO), 1736 (s, CO), 1597 (m, phenyl), 1506 (m, phenyl),

1471 (m), 1282 (m), 1204 (s), 1177 (m), 1133 (s, OCH_3), 1098 (m), 806 (m) cm^{-1}; **UV-Vis** ($CHCl_3$) λ_{max}/nm (ε/mol L^{-1} cm^{-1}): 420 (33579), 515 (1748), 550 (624), 589 (532), 645 (286); **elemental analysis** (%) calculated: C 70.44, H 5.32, N 5.48, found: C 70.51 H 5.45, N 5.56.

10,15,20-Tetra[3-(*R*,*R*,*R*,*R*)-2-*N*-dodecylamidoethyloxyphenyl]-porphyrin ((*R*,*R*,*R*,*R*)-2). Porphyrin (*R*,*R*,*R*,*R*)-**7** (100 mg, 98 mmol) was mixed with an excess of dodecylamine and the mixture heated to 80 °C. The mixture was allowed to react for about 16 h until no trace of starting material was left (control was done using TLC). The mixture was cooled and the dark red residue obtained was purified by column chromatography, obtaining 130 mg of (*R*,*R*,*R*,*R*)-**2** (79% yield) as a purple solid. Chromatography was carried out on silica gel with CH_2Cl_2–MeOH (100 : 1) mixture. **MF**: $C_{104}H_{146}N_8O_8$; **MW**: 1635.13; **LDI-TOF/MS** *m*/*z* (%): 1635.47 (100) $[M^+]$; **^{1}H NMR** (250 MHz, $CDCl_3$): 8.84 (s, 8H, pyrrole CH), 7.88 (d, J = 7.0, 4H, ArH), 7.79 (s, 4H, ArH), 7.67 (t, J = 7.2, 4H, ArH), 7.33 (d, J = 7.9, 4H, ArH), 6.64 (s, 4H, –CO*NH*–), 4.93 (q, J = 3.5, 4H, –O*CH*CH_3CONH–), 3.35–3.31 (m, 8H, –$CONHCH_2(CH_2)_{10}CH_3$), 1.70 (d, J = 6.4, 12H, $OCH*CH_3*CONH$), 1.57 (m, 8H, –$CONHCH_2*CH_2*(CH_2)_9CH_3$) 1.20–1.16 (m, 72H, –$CONHCH_2*(CH_2)_9*CH_3$), 0.85–0.80 (t, J = 6.4, 12H, –$CONHCH_2(CH_2)_{10}*CH_3*$), −2.8 (s, 4H, pyrrole NH) ppm; **FT-IR** (KBr): 3286 (w, NH), 2923 (s, CH_2), 2853 (s, CH_2), 1656 (s, CO), 1595 (m, phenyl), 1505 (w, phenyl), 1468 (s), 1237 (m), 1165 (m), 1082 (m), 801 (m) cm^{-1}; **UV-Vis** ($CHCl_3$) λ_{max}/nm (ε mol L^{-1} cm^{-1}): 420 (31090), 515 (1818), 549 (645), 589 (545), 645 (290) nm; **elemental analysis** (%) calculated: C 76.34, H 8.99, N 6.85, found C 76.18, H 9.52 N 6.64.

5,10,15,20-Tetra[3-(*R*,*R*,*R*,*R*)-2-*N*-octadecylamidoethyloxy-phenyl]porphyrin ((*R*,*R*,*R*,*R*)-3). Compound (*R*,*R*,*R*,*R*)-**3** was prepared using the same procedure as for (*R*,*R*,*R*,*R*)-**2**, using octadecylamine, and yielded 81% of the desired material. **MF**: $C_{128}H_{194}N_8O_8$; **MW**: 1971.50; **LDI-TOF/MS** *m*/*z* (%): 1971.89 (100) $[M^+]$; **UV-Vis** ($CHCl_3$) λ/nm (ε/mol L^{-1} cm^{-1}): 419 (28423), 515 (1781), 550 (644), 590 (536), 645 (285); **^{1}H NMR** (250 MHz, $CDCl_3$): 8.88 (s, 8H, pyrrole H), 7.92 (d, J = 7.1, 4H, ArH), 7.83 (s, 4H, ArH), 7.70 (t, J = 7.3, 4H, ArH), 7.40 (d, J = 7.9, 4H, ArH), 6.68 (s, 4H, –CO*NH*–), 4.97 (q, J = 3.4, 4H, –O*CH*CH_3CONH–), 3.36–3.34 (m, 8H, –$CONHCH_2(CH_2)_{16}CH_3$), 1.73 (d, J = 6.8, 12H, $OCH*CH_3*CONH$), 1.56 (m, 8H, –$CONHCH_2CH_2(CH_2)_{15}CH_3$), 1.24–1.21 (m, 128H, –$CONHCH_2*(CH_2)_{16}*CH_3$), 0.91–0.86 (t, J = 6.0, 12H, –$CONHCH_2(CH_2)_{16}*CH_3*$), −2.80 (s, 4H, pyrrole NH) ppm; **FT-IR** (KBr): 3286 (w, NH), 2923 (s, CH_2), 2852 (s, CH_2), 1655 (s, CO), 1602 (m, phenyl), 1502 (w, phenyl), 1467 (m), 1237 (m), 1176 (m), 1085 (m), 801 (m) cm^{-1}; **elemental analysis** (%) calculated: C 77.92, H 9.91, N 5.68, found: C 77.75, H 9.97, N 5.59.

5,10,15,20-Tetra[4-(*R*,*R*,*R*,*R*)-2-*N*-dodecylamidoethyloxyphenyl]-porphyrin ((*R*,*R*,*R*,*R*)-1). Compound (*R*,*R*,*R*,*R*)-**1** was prepared following the same procedure used for the synthesis of (*R*,*R*,*R*,*R*)-**2**. Porphyrin (*R*,*R*,*R*,*R*)-**8**[34] (100 mg, 98 mmol) was mixed with an excess of dodecylamine. Pure (*R*,*R*,*R*,*R*)-**1** was obtained as a purple solid (135 mg) (81% yield) after purification. **MF**: $C_{104}H_{146}N_8O_8$; **MW**: 1635.13; **LDI-TOF/MS** *m*/*z* (%): 1635.61 (100) $[M]^+$; **^{1}H NMR** (250 MHz, $CDCl_3$): 8.84 (s, 8H, pyrrole CH), 8.14 (d, J = 8.5, 8H, ArH), 7.30 (d, J = 8.7, 8H, ArH), 6.69 (t, J = 6.2, 4H, CONH), 4.99 (q, J = 6.8, 4H, –O*CH*CH_3CONH–), 3.47–3.38 (m, 8H, –$CONHCH_2(CH_2)_{10}CH_3$), 1.80 (d, J = 6.8, 12H, –$OCH*CH_3*CONH$–), 1.66–1.63 (m, 8H, –$CONHCH_2CH_2(CH_2)_9CH_3$), 1.36–1.16 (m, 72H, –$CONHCH_2CH_2*(CH_2)_9*CH_3$), 0.79 (t, J = 6.0, 12H, –$CONHCH_2CH_2(CH_2)_{15}*CH_3*$), −2.8 (s, 4H, pyrrole NH) ppm; **FT-IR** (KBr): 3286 (w, NH), 2924 (s, CH_2), 2853 (s, CH_2), 1656 (s, CO), 1606 (m, phenyl), 1505 (m, phenyl), 1468 (m), 1277 (w), 1236 (s), 1176 (m), 1082 (m), 801 (m) cm^{-1}; **UV-Vis** ($CHCl_3$) λ_{max}/nm (ε/mol L^{-1} cm^{-1}): 419 (34618), 515 (1290), 549 (818), 590 (418), 645 (436); **elemental analysis** (%) calculated: C 76.34, H 8.99, N 6.85, found: C 76.25, H 9.17, N 6.93.

AFM experiments

Solutions of the porphyrins in the different solvents were prepared by gentle warming prior to deposition of a drop on freshly cleaved graphite (ZYB grade). The AFM images were recorded on a PicoSPM (Molecular Imaging). The acoustic mode was used with resonance frequencies of the silicon tips (Nanosensors, FM type force constant 1.2–3.5 N m^{-1} and diameter 5 nm) of around 60–70 kHz. All the images were recorded under atmospheric conditions.

Acknowledgements

This work was supported by the European Union Marie Curie Research Training Network CHEXTAN (MRTN-CT-2004-512161), the Dirección General de Investigación, Ciencia y Tecnología (Spain, under the project CTQ2006-06333/BQU), and the DGR, Catalonia (Project 2005 SGR-00591). We warmly thank Amable Bernabé at the ICMAB for recording IR and LDI-TOF spectra.

References

1 J. C. Chambron, S. Chardonnoblat, A. Harriman, V. Heitz and J. P. Sauvage, *Pure Appl. Chem.*, 1993, **65**, 2343–2349.
2 A. Harriman and J. P. Sauvage, *Chem. Soc. Rev.*, 1996, **25**, 41–48.
3 J. C. Chambron, J. P. Collin, J. O. Dalbavie, C. O. Dietrich-Buchecker, V. Heitz, F. Odobel, N. Solladie and J. P. Sauvage, *Coord. Chem. Rev.*, 1998, **178**, 1299–1312.
4 M. Andersson, M. Linke, J. C. Chambron, J. Davidsson, V. Heitz, J. P. Sauvage and L. Hammarstrom, *J. Am. Chem. Soc.*, 2000, **122**, 3526–3527.
5 I. M. Dixon, J. P. Collin, J. P. Sauvage and L. Flamigni, *Inorg. Chem.*, 2001, **40**, 5507–5517.
6 L. Flamigni, A. M. Talarico, J. C. Chambron, V. Heitz, M. Linke, N. Fujita and J. P. Sauvage, *Chem.–Eur. J.*, 2004, **10**, 2689–2699.
7 L. Flamigni, V. Heitz and J. P. Sauvage, *Struct. Bonding*, 2006, **121**, 217–261.
8 G. Steinberg-Yfrach, P. A. Lidell, S.-C. Hung, A. L. Moore, D. Gust and T. A. Moore, *Nature*, 1997, **385**, 239–241.
9 J. A. Hutchison, T. D. M. Bell, T. Ganguly, K. P. Ghiggino, S. J. Langford, N. R. Lokan and M. N. Paddon-Row, *J. Photochem. Photobiol., A*, 2008, **195**, 220–225.
10 R. F. Kelley, J. L. Suk, T. M. Wilson, Y. Nakamura, D. M. Tiede, A. Osuka, J. T. Hupp and M. R. Wasielewski, *J. Am. Chem. Soc.*, 2008, **130**, 4277–4284.
11 J. Deisenhofer and H. Michel, *Chem. Scr.*, 1989, **29**, 203–220.

12 E. Tsuchida, T. Komatsu and J.-H. Fuhrhop, *Polym. Adv. Technol.*, 1998, **9**, 569–578.
13 M. C. Lensen, S. J. T. van Dingenen, J. A. A. W. Elemans, H. P. Dijkstra, G. P. M. van Klink, G. van Koten, J. W. Gerritsen, S. Speller, R. J. M. Nolte and A. E. Rowan, *Chem. Commun.*, 2004, 762–763.
14 Y. Nakamura, N. Aratani and A. Osuka, *Chem. Soc. Rev.*, 2007, **36**, 831–845.
15 R. van Hameren, A. M. van Buul, M. A. Castriciano, V. Villari, N. Micali, P. Schön, S. Speller, L. M. Scolaro, A. E. Rowan, J. A. A. W. Elemans and R. J. M. Nolte, *Nano Lett.*, 2008, **8**, 253–259.
16 Q. Guo, J. Yin, R. E. Palmer, N. Bampos and J. K. M. Sanders, *J. Phys.: Condens. Matter*, 2003, **15**, S3127–S3138.
17 A. Huijser, B. M. J. M. Suijkerbuijk, R. J. M. K. Gebbink, T. J. Savenije and L. D. A. Siebbeles, *J. Am. Chem. Soc.*, 2008, **130**, 2485–2492.
18 A. D. Schwab, D. E. Smith, B. Bond-Watts, D. E. Johnston, J. Hone, A. T. Johnson, J. C. de Paula and W. F. Smith, *Nano Lett.*, 2004, **4**, 1261–1265.
19 A. L. Yeats, A. D. Schwab, B. Massare, D. E. Johnston, A. T. Johnson, J. C. de Paula and W. F. Smith, *J. Phys. Chem. C*, 2008, **112**, 2170–2176.
20 J. S. Lindsey, *New J. Chem.*, 1991, **15**, 153–180.
21 D. Philp and J. F. Stoddart, *Angew. Chem., Int. Ed. Engl.*, 1996, **35**, 1154–1196.
22 P. N. W. Baxter, J.-M. Lehn, B. O. Kneisel, G. Baum and D. Fenske, *Chem.–Eur. J.*, 1999, **5**, 113–120.
23 F. J. M. Hoeben, P. Jonkheijm, E. W. Meijer and A. P. H. J. Schenning, *Chem. Rev.*, 2005, **105**, 1491–1546.
24 P. Jonkheijm, P. van der Schoot, A. P. H. J. Schenning and E. W. Meijer, *Science*, 2006, **313**, 80–83.
25 R. M. Capito, H. S. Azevedo, Y. S. Velichko, A. Mata and S. I. Stupp, *Science*, 2008, **319**, 1812–1816.
26 V. Palermo and P. Samori, *Angew. Chem., Int. Ed.*, 2007, **46**, 4428–4432.
27 E. Gomar-Nadal, J. Puigmartí-Luis and D. B. Amabilino, *Chem. Soc. Rev.*, 2008, **37**, 490–504.
28 I. Doudevski and D. K. Schwartz, *J. Am. Chem. Soc.*, 2001, **123**, 6867–6872.
29 N. Miyashita, H. Möhwald and D. G. Kurth, *Chem. Mater.*, 2007, **19**, 4259–4262.
30 P. Iavicoli, M. Linares, A. Pérez del Pino, R. Lazzaroni and D. B. Amabilino, *Superlattices Microstruct.*, 2008, **44**, 556–562.
31 T.-Q. Nguyen, M. L. Bushey, L. E. Brus and C. Nuckolls, *J. Am. Chem. Soc.*, 2002, **124**, 15051–15054.
32 J. Puigmartí-Luis, A. Minoia, A. Pérez del Pino, G. Ujaque, C. Rovira, A. Lledós, R. Lazzaroni and D. B. Amabilino, *Chem.–Eur. J.*, 2006, **12**, 9161–9175.
33 T. Ikeda, M. Asakawa, M. Goto, K. Miyake, T. Ishida and T. Shimizu, *Langmuir*, 2004, **20**, 5454–5459.
34 J. Otsuki, E. Nagamine, T. Kondo, K. Iwasaki, M. Asakawa and K. Miyake, *J. Am. Chem. Soc.*, 2005, **127**, 10400–10405.
35 M. Minguet, D. B. Amabilino, J. Cirujeda, K. Wurst, I. Mata, E. Molins, J. J. Novoa and J. Veciana, *Chem.–Eur. J.*, 2000, **6**, 2350–2361.
36 M. Minguet, D. B. Amabilino, J. Vidal-Gancedo, K. Wurst and J. Veciana, *J. Mater. Chem.*, 2002, **12**, 570–578.
37 A. D. Adler, *J. Org. Chem.*, 1967, **32**, 476.
38 M. Linares, P. Iavicoli, K. Psychogyiopoulou, D. Beljonne, S. De Feyter, D. B. Amabilino and R. Lazzaroni, *Langmuir*, 2008, **24**, 9566.
39 Y. Zhou, B. Wang, M. Zhu and J. G. Hou, *Chem. Phys. Lett.*, 2005, **403**, 140–145.
40 D. B. Amabilino, S. De Feyter, R. Lazzaroni, E. Gomar-Nadal, J. Veciana, C. Rovira, M. M. Abdel-Mottaleb, W. Mamdouh, P. Iavicoli, K. Psychogyiopoulou, M. Linares, A. Minoia, H. Xu and J. Puigmartí-Luis, *J. Phys.: Condens. Matter*, 2008, **20**, 184003.
41 D. B. Amabilino and J. Veciana, *Top. Curr. Chem.*, 2006, **265**, 253–302.